# Measurement of the proton spectrum from the $^2H(n,p)2n$ reaction at 13.98 MeV and the neutron-neutron scattering length*

R. C. Haight, S. M. Grimes, and J. D. Anderson
*Lawrence Livermore Laboratory, Livermore, California 94550*
(Received 20 September 1976; revised manuscript received 11 February 1977)

The spectrum of protons from the $^2H(n,p)2n$ reaction at $E_n = 13.98$ MeV has been measured at $\bar{\theta}_p = 1.6°$ with a magnetic-quadrupole-doublet charged-particle spectrometer. The experimental resolution of 200 keV is more than a factor of 2 improvement over that of previous measurements. The high energy peak in the proton spectrum due to the neutron-neutron final state interaction has been analyzed to yield a value of the neutron-neutron scattering length $a_{nn}$. Comparison of these data with an impulse approximation calculation and with exact three-body calculations indicates a value of $a_{nn}$ which is significantly more negative than the accepted value of $a_{nn} = -16.6 \pm 0.5$ fm.

[NUCLEAR REACTIONS $^2H(n,p)2n$, $E = 13.98$ MeV, $\bar{\theta}_p = 1.6°$; measured $\sigma(E_p)$; deduced $n$-$n$ scattering length.]

## I. INTRODUCTION

The neutron-neutron scattering length $a_{nn}$ is a quantity of fundamental importance in the nucleon-nucleon interaction. It parametrizes neutron-neutron scattering in the limit of low energies, and it can be compared with the nuclear part of the proton-proton scattering length in discussing the possible charge symmetry of nuclear forces.

One of the several methods to deduce this quantity is to measure the neutron-neutron ($n$-$n$) final state interaction (fsi) in the $^2H(n,p)2n$ reaction. In a kinematically incomplete experiment, the $n$-$n$ fsi enhances the highest energy component of the proton spectrum near $\theta_p = 0°$. In this region of the three-body phase space, the two remaining neutrons have a low relative momentum and hence a large fsi.

The proton spectrum at 0° from this reaction therefore exhibits a peak at the highest allowed $E_p$ due to the $n$-$n$ fsi. The width of this peak depends on the details of the nucleon-nucleon interactions and in particular on the value of $a_{nn}$. The intrinsic full width at half maximum (FWHM) of the peak is in the range 300 to 700 keV regardless of incident neutron energy if $a_{nn}$ is in the (expected) range of $-24$ to $-16$ fm. Davis *et al.*[1] have shown that the experimental resolution must be considerably better than the intrinsic width for a good determination of $a_{nn}$ with reasonable statistics.

The best experimental resolution obtained previously is, to our knowledge, 440 keV by Shirato *et al.*[2] The resolution in all other previous measurements is significantly worse. For resolutions greater than 400 keV, the results of Ref. 1 show that the instrumental resolution must be well known indeed to distinguish between the reasonable but widely differing values of $a_{nn} = -16$ and $a_{nn} = -24$ fm. The previous measurements on this reaction and other determinations of $a_{nn}$ have recently been summarized by Kühn.[3]

We have performed a new measurement of the proton spectrum from the $^2H(n,p)2n$ reaction with a significantly improved instrumental energy resolution, namely, 200 keV, which is an improvement of more than a factor of 2 over the best previous value. For the first time, the instrumental resolution is less than the lowest anticipated natural width of the fsi peak. The improved resolution was made possible by the development of a new magnetic-quadrupole-doublet charged-particle spectrometer for neutron-induced reactions.[4] This spectrometer also enhances the signal-to-background ratio significantly.

The new results have been analyzed with the impulse approximation and with an exact calculation based on the Faddeev equations. The first analysis gives a value of $a_{nn} = -28 \pm 3$ fm which is surprisingly more negative than previous experiments, with poorer resolution, have indicated. Comparison of the new results with the exact calculations does not indicate such a negative value. Our value of $a_{nn}$ ($-23$ fm) based on these calculations does imply, however, that $a_{nn}$ is much closer to the value of $a_{np}$ ($-24$ fm) than to the Coulomb-corrected value of $a_{pp}$ ($-17.1 \pm 0.2$ fm) or to the presently accepted value of $a_{nn}$ ($-16.6 \pm 0.5$ fm).[3]

## II. EXPERIMENTAL METHOD

The improved resolution of this experiment was made possible by two technological advances. First, the availability of an intense neutron source allowed the use of thin deuterated radiators.

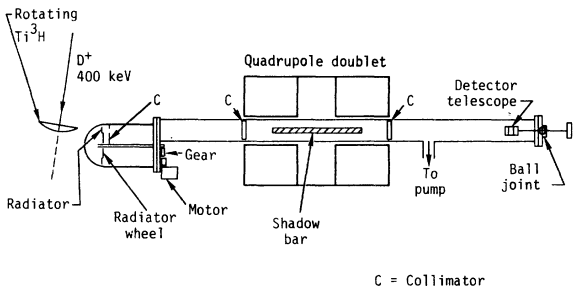


FIG. 1. Schematic layout of the experiment (not to scale). Collimator locations are denoted by C.

Second, a charged-particle magnetic-quadrupole spectrometer developed for neutron-induced reactions permitted detectors of good energy resolution to function well with the intense source and the backgrounds it produces.

The spectrometer consists basically of a magnetic-quadrupole-doublet lens which focuses the charged-particle reaction products from the radiator onto a silicon surface-barrier counter telescope. The solid angle is thereby enhanced significantly over the geometrical solid angle. On the other hand, neutrons and $\gamma$ rays produced near the source are of course not focused onto the detector. The result is a large increase in the signal-to-background ratio. The experimental layout is given schematically in Fig. 1.

Details of the measurement follow.

### A. Neutron source

Neutrons of 13.98 MeV were produced by the LLL rotating target neutron source (RTNS).[5] This source consists of a high-current accelerator, which produces a 400-keV deuteron beam of up to 20 mA, and a rotating tritiated titanium target backed by a thin (1.5 mm) copper alloy. The titanium layer of 5 mg/cm$^2$ is thick enough to stop the 400-keV deuteron beam. Neutrons produced by the $^3$H$(d,n)^4$He reaction at $\theta_n = 98°$ to the incident deuteron beam have an energy of 13.98 MeV and a minimum energy spread due to the changing deuteron energy as this beam slows down and stops in the Ti$^3$H layer. The energy spread of the neutrons is discussed in detail below. The maximum source strength used in these experiments was $2.3 \times 10^{12}$ neutrons/sec into $4\pi$ sr.

As shown in Fig. 1, the neutrons that travel directly from the neutron source to the radiator pass rather obliquely through the spherical surface of the rotating target. The materials between the source and the deuterated foil therefore constitute 0.39 mean-free paths or an attenuation of 32% for 13.98-MeV neutrons. Neutrons produced by the source at almost any other angle ($\theta_n < 82°$ or $\theta_n > 98°$) pass through much less material and hence are scattered less.

The neutron spectrum at the radiator could have been contaminated in two ways: First, 14-MeV neutrons, scattered elastically in the materials of the rotating target could have been incident at some nonzero angle to the normal of the radiator foil. Compared with the neutrons incident normally, these scattered neutrons would produce protons of lower energy from the $^1$H$(n,p)n$ and $^2$H$(n,p)2n$ reactions. Secondly, neutrons from the source could have been scattered and therefore not be at 13.98 MeV when they reached the radiator. Most of these neutrons will have lower energy and, even if they are incident normal to the radiator, will produce lower energy protons for the interaction with $^1$H and $^2$H. There may also be some neutrons with energies higher than 13.98 MeV. These neutrons are produced in the forward direction by the $^3$H$(d,n)$ reaction [$E_n$(max) = 15.6 MeV at 0°] and then elastically scattered toward the radiator by materials of the rotating target.

Measurement of the proton recoil spectrum from a $C^1H_2$ radiator showed that the contamination of the neutron spectrum was negligible for these measurements: For example, Fig. 2 shows the proton recoil spectrum near the elastic $n$-$p$ peak. Any contamination by neutrons near 14 MeV would be indicated by high or low energy tails on the peak. None is observed to below 5% of the peak height.

The contamination by neutrons which would give $^1$H$(n,p)$ protons in this region of the $n$-$n$ fsi peak in the $^2$H$(n,p)$ spectrum is also negligible: Contamination (counts per MeV)/elastic (total counts) $\approx 0.007$/MeV. For the small $^1$H impurity in the $C^2H_2$ radiator this effect would increase the measured $^2$H$(n,p)$ cross section by less than 0.1 mb sr$^{-1}$ MeV$^{-1}$.

### B. $C^2H_2$ radiator

The target for the neutrons was a 1.5-mg/cm$^2$ foil of $C^2H_2$. To distinguish this target from the rotating Ti$^3$H target, we call the $C^2H_2$ foil or other foils in this position, the "radiator." The $C^2H_2$ foil was one of up to 10 foils which could successively be placed in the radiator position by rotation of a radiator foil wheel. The radiator foils were 19 cm from the neutron source in an evacuated reaction chamber.

The $C^2H_2$ foil was prepared according to the method of Bartle and Meyer.[6] The ratio of normal hydrogen to deuterium in the foil was 0.04. The thickness and uniformity were determined by the energy loss of 5.5-MeV $\alpha$ particles passing through it. To restrict the angular acceptance

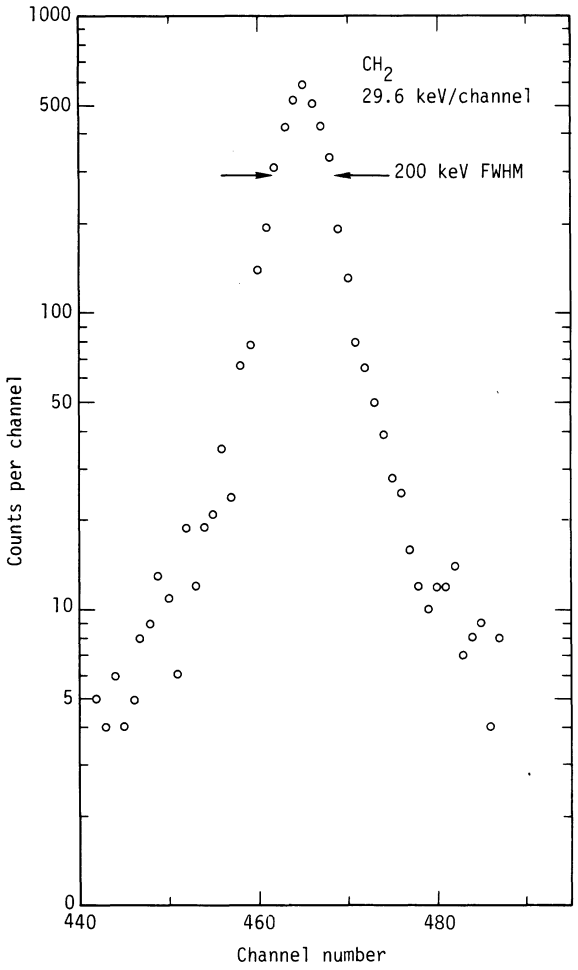


FIG. 2. Proton spectrum from a 1.2-mg/cm$^2$ $C^1H_2$ radiator.

($\Delta\theta_n$) from the neutron source, the width of the foil was only 1.1 cm. The foil height was 2.5 cm.

### C. Charged Particle spectrometer

Charged particles from the radiator were analyzed by a magnetic-quadrupole-doublet spectrometer.[4] The charged particles which passed through the various lead collimators, denoted C in Fig. 1, were focused by a magnetic-quadrupole-doublet lens onto a detector telescope 3.74 m from the radiator. A copper shadow bar 2.5 cm in diameter by 25 cm long in the center of the magnet shielded the telescope from the neutron source. The other collimators prevented charged particles produced by nuclear reactions in the beam tube walls from reaching the detector. These collimators had thicknesses of from 1 to 6 mm and were not intended to be thick to neutrons.

The detector telescope consisted of two silicon surface-barrier detectors, the $\Delta E$ detector being 167 $\mu$m thick by 300 mm$^2$ and the $E$ detector 1500 $\mu$m thick by 200 mm$^2$. The detector areas were collimated to 254 and 176 mm$^2$, respectively, for these experiments. Conventional electronics and particle identification techniques were used to identify the protons and to measure their energies.

The detector telescope was mounted on a rod which extended outside the evacuated region through a ball joint. This construction allowed mechanical movement of the telescope to the magnetic focal point for the charged particles. A $^{244}$Cm plus $^{238}$Pu $\alpha$ source was placed at the position of the radiator to indicate this focal point during alignment of the spectrometer.

The radiator, collimators, shadow bar, and detector telescope were all housed in a vacuum system which was maintained at a pressure of about 1.3 Pa (10 $\mu$m of Hg) with a mechanical pump. The detectors functioned well at this pressure and the hydrogen-containing gases were sufficiently rarefied to contribute negligibly to the background. Wherever it was necessary, the aluminum and stainless steel metals of the vacuum system were covered with 1 mm of lead to stop protons from $(n,p)$ reactions from reaching the detectors. The cross section for $(n,p)$ reactions on lead is approximately two orders of magnitude less than those cross sections on aluminum or stainless steel.

### D. Acceptance of the spectrometer

The important characteristic of the magnetic-quadrupole-doublet lens is its focusing action which enhances the solid angle for detecting charged particles over the geometric solid angle of the detector telescope. The lens also acts as an energy-bandpass filter. These two effects may be described by defining an effective solid angle $\Delta\Omega(E_p, b_1, b_2)$ which is a function of the proton energy and the magnetic field gradients $b_1$ and $b_2$ in the two lenses. The total acceptance $a(E_p, b_1, b_2)$ of the spectrometer is then the product of the effective solid angle and the efficiency $\epsilon(E_p)$ of the detector telescope and its associated electronics,

$$a(E_p, b_1, b_2) = \Omega(E_p, b_1, b_2)\epsilon(E_p). \quad (1)$$

In practice only the acceptance needs to be known. It was measured by observing the spectrum of protons from a thick (3.2 mm) $CH_2$ radiator. The shape of this spectrum emerging from the radiator is easily shown to be inversely proportional to the stopping power $dE_p(E_p)/dx$ for protons in $CH_2$. The acceptance of the spectrometer therefore can be found from the spectrum observed with the spectrometer from the equality

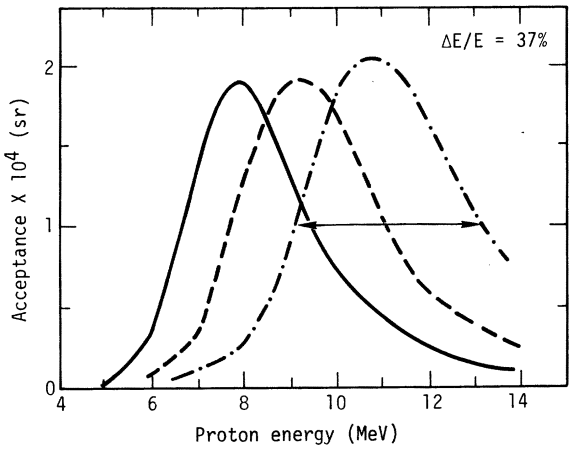


FIG. 3. Acceptance of the spectrometer for protons at three magnet settings.

$$\frac{dN_p}{dE_p}(E_p, b_1, b_2) = \Phi_n A\left[\frac{dE_p}{dx}(E_p)\right]^{-1}\frac{d\sigma}{d\Omega}(E_n, \theta_p)N_H\, a(E_p, b_1, b_2), \quad (2)$$

where $\Phi_n$ is the fluence of neutrons on the radiator (i.e., neutrons/cm$^2$), $A$ is the area of the radiator, the stopping power for protons in $CH_2$ is conveniently expressed as MeV cm$^2$/mg, $d\sigma/d\Omega(E_n, \theta_p)$ is the laboratory differential cross section at neutron energy $E_n$ for $n$-$p$ scattering at a proton recoil angle of $\theta_p$, and $N_H$ is the number of hydrogen atoms per mg of $CH_2$. Energy straggling and small angle multiple scattering of the protons in the $CH_2$ have negligible effect on the validity of Eq. (2). The stopping powers of Janni[7] were used to solve Eq. (2) for $a(E_p, b_1, b_2)$. To the number of significant figures given, these stopping powers are identical to those of Northcliffe and Schilling.[8]

The spectrometer acceptance measured in this way at three different magnet settings is shown in Fig. 3. The bandwidth for this combination of detector areas and source-to-detector separation is 37% FWHM which allowed measurement of proton spectra from 7 to 14 MeV with only three magnet settings.

The dimension of the acceptance is steradians. The values of Fig. 3 should therefore be compared with the geometrical solid angle subtended by a 176-mm$^2$ collimator at a distance of 3.74 m from the radiator. This solid angle is $1.3 \times 10^{-5}$ sr. The quadrupole has therefore increased the effective solid angle by a factor of about 15 at the center of the bandpass. With a smaller radiator, the enhancement would have been greater due to the decrease in off-axis sources. Measurement with a 6-mm diameter $\alpha$ source yielded an enhancement factor of 30. For detectors of smaller area used with this $\alpha$ source, enhancement factors of 200 have been observed. The bandwidths in these cases are reduced, however.

### E. Angular range accepted

The calculated distribution of reaction angles sampled in these measurements is shown in Fig. 4 for the center of the bandpass and for energies on the higher and lower sides where the acceptance is half its maximum value. The calculation assumed a neutron source 10 mm high by 1 mm wide as seen by the radiator. This size determined the range of incident neutron angles on any one element of the radiator. The range of proton angles emerging from this element and accepted by the spectrometer was calculated from a charged-particle transport code.[9] The combined $^2H(n,p)$ reaction angle was then calculated and averaged over the area of the radiator by numerical integration.

The angular range accepted is significantly smaller than that of preceding experiments (e.g., Ref. 2 and experimental references therein). The fsi peak cross section is somewhat larger therefore because the average angle is closer to 0°. The peak is also intrinsically narrower because of the smaller kinematic shift over the measured angular range.

This narrow angular range avoids a possible problem with this type of spectrometer, namely, the rather complicated energy-angle correlated

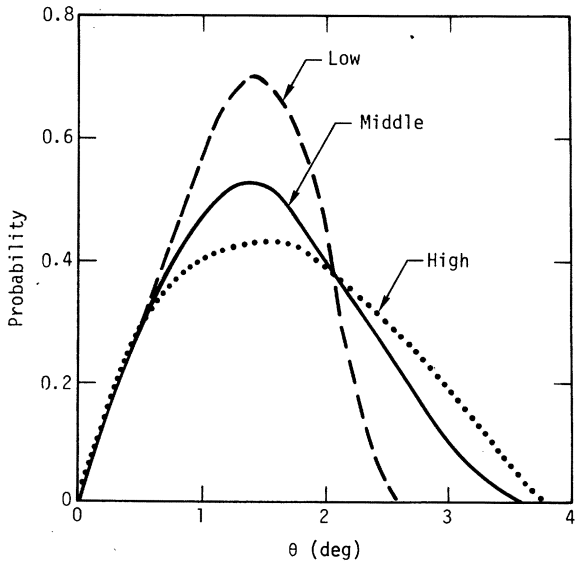


FIG. 4. Angular range sampled at the middle of the bandpass, and at the half maxima on the high and low sides of the bandpass. The relative probabilities are normalized to an integrated value of unity.

TABLE I. Contributors to the total energy resolution.

| | Contributor | $\Delta E$ (keV) | Comment |
|---|---|---|---|
| Neutron energy spread | $dE_n/dE_d$ | ~10 | |
| | $dE_n/d\theta[^3\mathrm{H}(d,n)]$ | 53 | Assuming no multiple scattering and $\overline{E}_d = 200$ keV |
| Proton energy spread | $dE_p/dx$ | 50 | $E_p = 14$ MeV in $C^1H_2$ radiator |
| | | | in $C^2H_2$ radiator |
| | | 65 | $E_p = 11.7$ MeV |
| | $dE_p/d\theta_{(n,p)}$ | 15 | $^1\mathrm{H}(n,p)$ |
| | | 15 | $^2\mathrm{H}(n,p)$ |
| Electronics | | ~40 | |
| Sum in quadrature | | 85 | $^1\mathrm{H}(n,p)$ protons at 14 MeV |
| | | 95 | $^2\mathrm{H}(n,p)$ protons at 11.7 MeV |
| Missing contribution | | 181 | For $^1\mathrm{H}(n,p)$ protons at 14 MeV |

acceptance as illustrated by the different curves in Fig. 4. The range is sufficiently small that the theoretical three-body calculations, reported in Sec. IV, give essentially the same angle-averaged spectrum independent of whether the distribution of angles is taken from the "middle," "high," or "low" curves of Fig. 4, or, in fact, from curves (not shown in Fig. 4) for the tails of the acceptance function. In the $\chi^2$ per degree freedom, discussed below, the differences are less than 0.01.

### F. Energy resolution and calibration

The energy resolution of the spectrometer was determined for protons by using a thin 1.2-mg/cm$^2$ $CH_2$ radiator. The length and width of this foil were identical to those of the $C^2H_2$ radiator. The spectrum of elastically scattered protons is shown in Fig. 2.

The known contributions to the measured 200 keV FWHM are listed in Table I. The sum, in quadrature, of these components is 85 keV. The missing contribution is then 181 keV.

We attribute this missing component to the energy spread of the neutrons incident on the radiator. The spread is due to two cooperating effects—the small-angle scattering of the deuteron beam in the $Ti^3H$ target of the neutron source and $dE_n/d\theta$ which is nearly maximal at $\theta_n = 98°$. A root mean squared scattering angle of only $\langle\theta_d^2\rangle^{1/2} = 5°$ in slowing down from 400 to 200 keV is sufficient to produce the observed energy spread. The average deuteron energy for the $^3\mathrm{H}(d,n)$ reaction is near 200 keV.

To verify this hypothesis, we measured the energy resolution of the source at lower deuteron beam energies where the values of $\langle\theta_d^2\rangle^{1/2}$ and $dE_n/d\theta$ are less. Energy spreads of 100 and 155 keV (± 20 keV) were measured at $E_d = 200$ and 300 keV, respectively. These values are consistent with a width of 120 keV at $E_d = 175$ keV which was determined by Bormann and Riehle[10] by an entirely different method. The exact neutron energy width at $E_d = 400$ keV, however, cannot be extrapolated from the measurements at lower energy because it depends on the tritium depth distribution in the $Ti^3H$ target which in turn depends strongly on the history of the target.[11]

To verify the resolution for the $C^2H_2$ radiator, deuterons from elastic $n$-$^2$H scattering were measured simultaneously with the breakup protons. The spectrum of deuterons is shown in Fig. 5. The statistics of this measurement are relatively poor because the deuterons were far from the bandpass center. Their trajectories correspond to those of 25-MeV protons. Nevertheless, a resolution for deuterons of 210 keV FWHM can be extracted from this spectrum. This resolution is expected to be somewhat larger than that for protons because of the larger $dE/dx$ in the radiator, i.e., 100 keV as opposed to 65 keV for protons. When added in quadrature to the "missing contribution," the expected resolution for deuterons is 212 keV which agrees remarkably well with the observed value of 210 keV.

A good energy calibration is required in this experiment to determine the width of the $n$-$n$ fsi peak. Seven calibration peaks that span the range

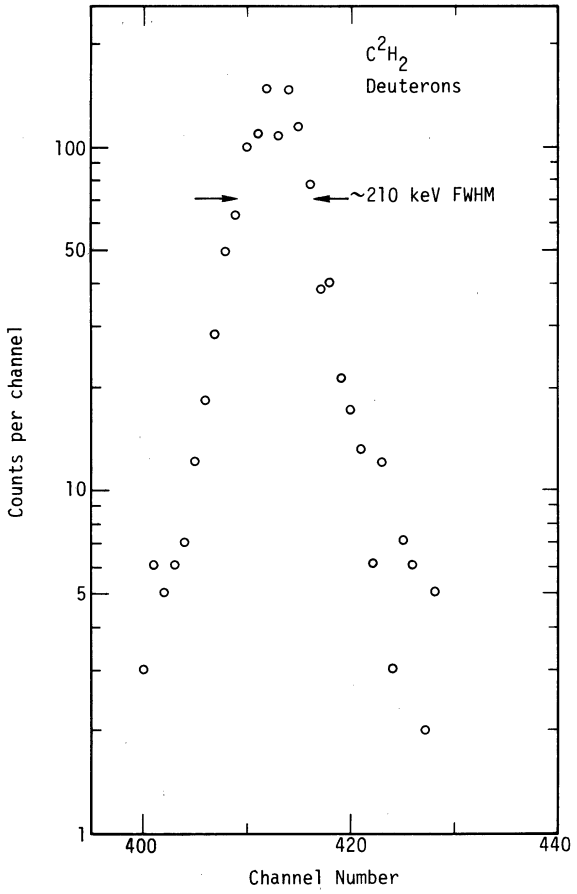


FIG. 5. Deuteron spectrum from the 1.5-mg/cm$^2$ $C^2H_2$ radiator.

8.2 to 14 MeV were used in this calibration. They were as follows: $^1H(n,p)$, $^2H(n,d)$, $^{27}Al(n,p_0)^{27}Mg$, $^{27}Al(n,p_2)^{27}Mg^*$ (1.69 MeV), $^{27}Al(n,p_3)^{27}Mg^*$ (1.94 MeV), $^{19}F(n,p_2)^{19}O^*$ (1.472 MeV), and $^{19}F(n,d_0)^{18}O$. The peaks from these calibration lines lie on a straight line on an energy vs channel number plot to within the experiment errors.

### G. Background

The background was measured by removing the radiator foil. In this case the spectrometer detected protons from $(n,p)$ reactions on the lead liners and collimators, $(n,p)$ reactions in impurities in the spectrometer, and $Si(n,p)$ reactions in the counters of the telescope. The "radiator out" and "radiator in" spectra for the magnet settings which focused the highest energy $^2H(n,p)$ protons are given in Fig. 6. The $^1H(n,p)$ peak comes from residual hydrogen in the spectrometer (in both spectra) as well as from the $^1H$ contaminant of the $C^2H_2$ radiator (in the radiator in spectrum).

For all measurements, including those on the $C^2H_2$, $CH_2$, Al, and $CF_2$ radiators, backgrounds were subtracted before the data were further analyzed.

## III. RESULTS

The double differential cross section for the $^2H(n,p)2n$ reaction at $\bar{\theta}_p = 1.6°$ is given in Table II and Fig. 7(a) and is replotted in Figs. 7(b), 9(a), and 9(b). The errors are statistical and include statistics in the foreground and background spectra and in the normalizing spectra from the thick $C^1H_2$ radiator.

The overall normalization of these data is uncertain to an additional ± 8% from three effects. The uncertainty in the thickness of the $C^2H_2$ radiator is ± 7%. The normalization of the stopping powers has been estimated[12] to be uncertain to less than 3%. Finally, the uncertainty in the $n$-$p$ elastic differential cross section is less than 1.6%.[13]

## IV. ANALYSIS

The present results have been analyzed in two ways to extract the $n$-$n$ scattering length. It is important to bear in mind that different model-dependent analyses of these data can give different values of $a_{nn}$. We have, therefore, extracted values of $a_{nn}$ according to two different models both to emphasize the model dependence of the result and also to facilitate comparison of these data with those obtained by other authors.

### A. Impulse approximation calculation

The impulse approximation as formulated by Phillips[14] was first used to extract $a_{nn}$. This for-

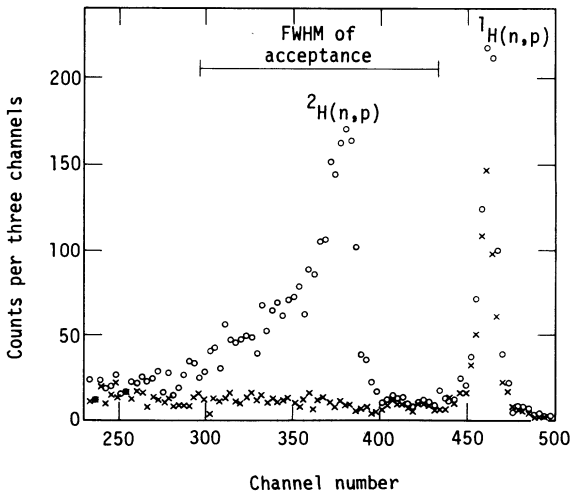


FIG. 6. Raw spectrum of protons from a $C^2H_2$ radiator not corrected for the energy dependent acceptance of the spectrometer.

TABLE II. Experimental proton energy spectrum from the $^2H(n,p)2n$ reaction at $E_n = 13.95$ MeV and $\bar{\theta} = 1.6°$. The errors are statistical as described in the text.

| $E_p$ (MeV) | $\frac{d^2\sigma}{d\Omega dE}$ (mb sr$^{-1}$ MeV$^{-1}$) | $\frac{\Delta d^2\sigma}{d\Omega dE}$ (mb sr$^{-1}$ MeV$^{-1}$) | $E_p$ (MeV) | $\frac{d^2\sigma}{d\Omega dE}$ (mb sr$^{-1}$ MeV$^{-1}$) | $\frac{\Delta d^2\sigma}{d\Omega dE}$ (mb sr$^{-1}$ MeV$^{-1}$) |
|---|---|---|---|---|---|
| 6.14 | 14.20 | 5.57 | 9.24 | 6.07 | 0.82 |
| 6.22 | 8.22 | 3.52 | 9.33 | 5.29 | 0.88 |
| 6.31 | 18.30 | 4.56 | 9.42 | 8.58 | 0.96 |
| 6.40 | 8.50 | 3.85 | 9.51 | 5.24 | 0.90 |
| 6.49 | 8.26 | 3.34 | 9.60 | 7.75 | 0.92 |
| 6.58 | 10.20 | 2.94 | 9.69 | 7.93 | 0.89 |
| 6.67 | 5.36 | 1.60 | 9.78 | 6.27 | 0.86 |
| 6.76 | 11.70 | 2.60 | 9.87 | 6.28 | 0.86 |
| 6.85 | 5.69 | 2.58 | 9.95 | 7.70 | 0.87 |
| 6.94 | 12.00 | 2.29 | 10.04 | 5.46 | 0.80 |
| 7.02 | 6.70 | 2.19 | 10.13 | 6.87 | 0.82 |
| 7.11 | 8.95 | 1.81 | 10.22 | 8.42 | 0.89 |
| 7.20 | 7.84 | 1.78 | 10.31 | 7.40 | 0.90 |
| 7.29 | 8.00 | 1.76 | 10.40 | 7.58 | 0.84 |
| 7.38 | 8.33 | 1.65 | 10.49 | 8.55 | 0.93 |
| 7.47 | 10.30 | 1.51 | 10.58 | 10.90 | 0.96 |
| 7.56 | 11.30 | 1.69 | 10.66 | 11.00 | 1.00 |
| 7.65 | 6.64 | 1.33 | 10.75 | 9.44 | 0.96 |
| 7.73 | 6.36 | 1.26 | 10.84 | 12.70 | 1.06 |
| 7.82 | 8.53 | 1.34 | 10.93 | 12.60 | 1.01 |
| 7.91 | 8.84 | 1.41 | 11.02 | 14.60 | 1.20 |
| 8.00 | 7.04 | 1.26 | 11.11 | 14.90 | 1.20 |
| 8.09 | 8.45 | 1.26 | 11.20 | 18.60 | 1.34 |
| 8.18 | 7.37 | 1.18 | 11.29 | 21.20 | 1.39 |
| 8.27 | 7.15 | 1.13 | 11.38 | 23.60 | 1.52 |
| 8.36 | 5.38 | 1.05 | 11.46 | 26.60 | 1.64 |
| 8.44 | 7.31 | 1.08 | 11.55 | 27.30 | 1.63 |
| 8.53 | 4.88 | 0.94 | 11.64 | 16.70 | 1.31 |
| 8.62 | 6.32 | 1.03 | 11.73 | 7.46 | 0.93 |
| 8.71 | 8.41 | 1.07 | 11.82 | 1.70 | 0.62 |
| 8.80 | 7.09 | 1.03 | 11.91 | 1.61 | 0.57 |
| 8.89 | 7.90 | 1.04 | 12.00 | 1.11 | 0.45 |
| 8.98 | 4.10 | 0.95 | 12.09 | 1.01 | 0.53 |
| 9.07 | 7.48 | 0.97 | 12.17 | 1.30 | 0.74 |
| 9.16 | 7.57 | 0.90 | 12.26 | −0.23 | 0.63 |

mulation is simply a plane-wave Born approximation to the reaction amplitude with the additional assumption that the knock-out $n$-$p$ interaction is a $\delta$ function in configuration space. The impulse approximation does include, however, the extended structure of the deuteron. In contrast to the Watson-Migdal theory,[15,16] the impulse approximation includes the effective range of the $n$-$n$ interaction as well as an explicit form for the deuteron wave function. Both of these formulations contain only one term of the infinite rescattering series, however.

Numerical evaluations of Eqs. (14) and (15) of Ref. 14 were performed with the code of Davis[1] for different values of $a_{nn}$. The two parameters of this calculation, namely, the $n$-$n$ effective range $r_{nn}$ and the boundary radius $r$, were taken to be $r_{nn} = 2.794$ fm and $r = 1.0$ fm. Reasonable variations of $r_{nn}$ do not have significant effect on the results as noted previously by Shirato, Saitoh, and Koori.[17] Varying $r$ has little effect if $r \leq 1.6$ fm. To within a normalization constant, this calculation should describe the $n$-$n$ fsi peak.

In addition to the fsi peak there is a smooth continuum extending to low proton energies. Following the form used by Shirato *et al.*,[2] we include a term proportional to $k_p q^3$ where $k_p$ is the laboratory proton wave number and $q$ is the relative wave number of the two neutrons.

The experimental data were fitted by a linear combination of the impulse approximation calculation and the $k_p q^3$ term. Before fitting, both terms were smeared with the experimental resolution function derived from elastic $n$-$p$ scattering, Fig.

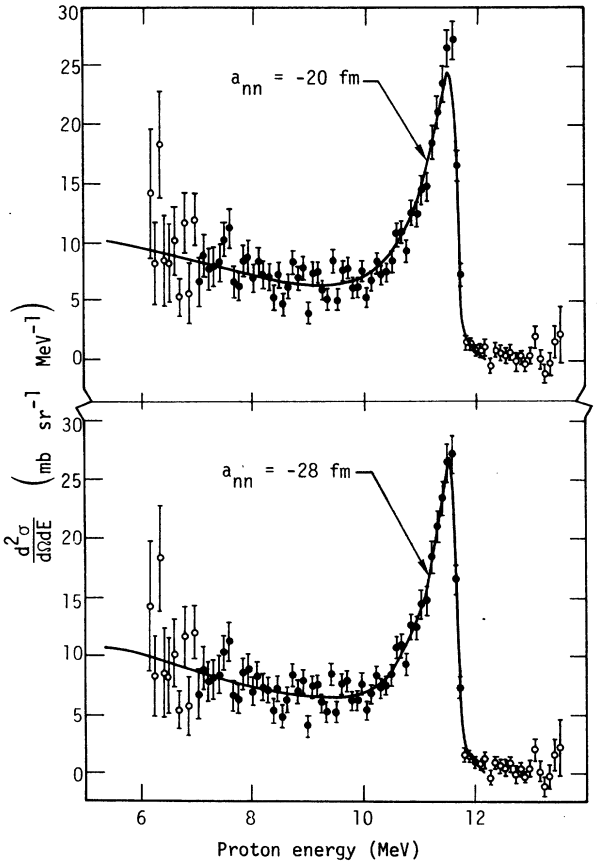


FIG. 7. Double differential cross section for the reaction $^2H(n,p)2n$, at $E_n = 13.98$ MeV and $\theta_p = 1.6°$. The solid circles denote the data used in the least-squares fit. The other data are denoted by open circles. The curves are calculations based on the impulse approximation plus a term proportional to $k_p q^3$. The impulse approximation was calculated with (a) $a_{nn} = -28$ fm and (b) $a_{nn} = -20$ fm.

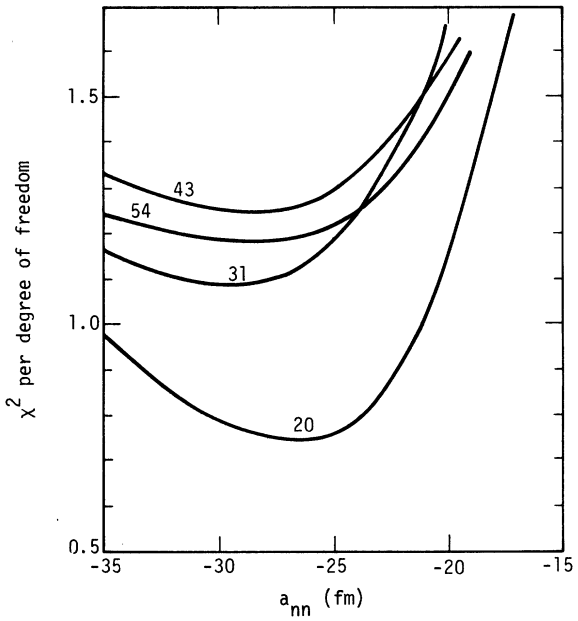


FIG. 8. $\chi^2$ per degree of freedom vs $a_{nn}$ for the calculations with the impulse approximation plus $k_p q^3$ background.

2. The coefficients of each term were determined to give a minimum $\chi^2$ fit.

Two fits with different values of $a_{nn}$ are shown in Figs. 7(a) and 7(b). The points from $E_p = 7.0$ to 11.8 MeV were included in the fits. They are denoted by the solid circles in Fig. 7. It is obvious that the fit with $a_{nn} = -28$ fm describes the data much better than that with $a_{nn} = -20$ fm. The shape and particularly the width of the fsi peak are the determining factors.

For other values of $a_{nn}$ the values of $\chi^2$ per degree of freedom are plotted in Fig. 8. The integer $N$ on each curve denotes the number of points used in the fit. The corresponding energy regions are 7.0 to 11.8 MeV ($N = 54$), 8.0 to 11.8 MeV ($N = 43$), .9.0 to 11.8 MeV ($N = 31$), and 10.0 to 11.8 MeV ($N = 20$). For each of these regions the minimum $\chi^2$ is between $a_{nn} = -26$ and $-29$ fm. Clearly excluded in this analysis are values of $|a_{nn}| \leq 20$ fm.

### B. Exact three-body calculation

Results of an exact calculation based on the Faddeev equations were kindly sent to us by Kloet.[18] These calculations which can use local potentials have been previously described.[19] For the singlet nucleon-nucleon interaction, two different potentials were used, namely, the Reid soft-core (RSC) potential,[20] and the Malfliet-Tjon (MT13) potential.[21,22] These potentials have the interesting difference that $a_{nn} = -17.1$ fm in the former and $a_{nn} = -23.7$ fm in the latter. In the triplet state, the MT13 potential was used. The calculations were done with the assumption that the interactions are charge independent. Furthermore, only $S$-wave interactions were included.

The calculations were smeared with the experimental resolution function (Fig. 2), shifted slightly to compensate for the small difference in incident neutron energy (14.4 MeV in the calculation), and then normalized with one constant to fit the measured spectrum. The results are shown in Fig. 9 where the data between $E_p = 7.0$ and 11.8 MeV have been fitted. Values of $\chi^2$ per degree of freedom are summarized in Table III for four subsets of the experimental data. The constants that multiply the calculation are also given in the table. The region between $E_p = 10.0$ and 11.8 MeV of course emphasizes the $n$-$n$ fsi region the most.

These results show that the calculation with the MT13 singlet interaction describes the $n$-$n$ fsi peak much better than that with the Reid soft-core singlet potential. In particular, both the height and shape of the fsi peak are better described.

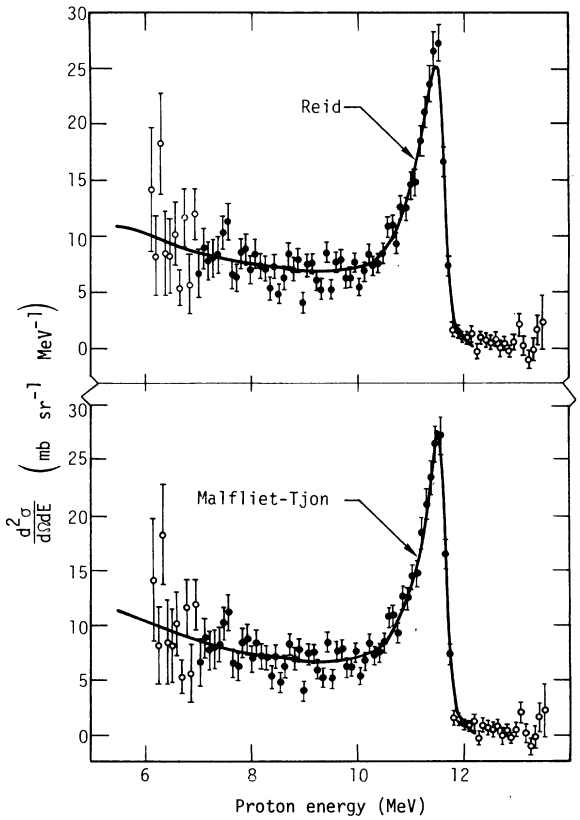


FIG. 9. Experimental data of Fig. 7 replotted. Calculations from Ref. 18 are (a) with Reid potential and (b) with Malfliet-Tjon potential.

TABLE III. $\chi^2$ per degree of freedom and normalization for the two exact calculations. The form of the nucleon-nucleon singlet interaction, Reid or Malfliet-Tjon (MT13), denotes the calculation.

| Region fit (proton energy MeV) | Number of points | $\chi^2$ per degree of freedom | | Normalization | |
|---|---|---|---|---|---|
| | | Reid | MT13 | Reid | MT13 |
| 10.0 to 11.8 | 20 | 1.13 | 0.98 | 1.287 | 1.289 |
| 9.0 to 11.8 | 31 | 1.29 | 1.18 | 1.274 | 1.278 |
| 8.0 to 11.8 | 43 | 1.48 | 1.38 | 1.256 | 1.261 |
| 7.0 to 11.8 | 54 | 1.36 | 1.29 | 1.258 | 1.264 |

The extraction of $a_{nn}$ from these comparisons of the data with the exact calculations is not straightforward. In the first place, other parameters (such as those describing the form of the two-body potential) enter the calculation. Although the dominant sensitivity of the calculations is to $a_{nn}$ in the fsi region, other parameters could influence the calculated spectrum to some degree. Unfortunately a systematic investigation of the effects of of these other parameters with the most advanced three-body codes is beyond our present capabilities. Secondly, one has the choice of comparing theory and experiment over a small region which includes the $n$-$n$ fsi or over the whole range spanned by the experiment. The fsi peak is most sensitive to $a_{nn}$ but, on the other hand, the exact calculation should describe the complete spectrum.

In view of these limitations, we make an arbitrary choice and two assumptions to interpret the experimental results. The choice is that, for the purposes of extracting $a_{nn}$, we normalize the calculations to experiment over a large energy range and then compare theory and experiment at the peak of the fsi, namely, at the two highest experimental points. The assumptions are that the peak height of the calculation depends only on $a_{nn}$ and the dependence over the small range $17 \leq |a_{nn}| \leq 25$ fm is linear. The result is then that $a_{nn} = -24.4 \pm 3.2$ fm if the calculations are normalized to the data between 7.0 and 11.8 MeV. If instead the normalization is done between 10.0 and 11.8 MeV, $a_{nn} = -23.2 \pm 3.6$ fm.

We emphasize that these values of $a_{nn}$ are obtained only with a most naive approach. Further, theoretical calculations should be made to shed light on the assumptions made.

## V. DISCUSSION

Analyses of these good resolution data with both exact calculations and with the impulse approximation indicate an $n$-$n$ scattering length that is significantly more negative than the generally accepted value of $a_{nn} = -16.6 \pm 0.5$ fm.[3] One might infer from this result that these new data disagree with previous measurements. Such is not always the case, however. If the data of Ref. 2, for example, are analyzed in the same way as we have done here with their *measured* resolution function, the results agree with those of the present measurement.

One possible explanation of the discrepancy is that there is some difficulty with the exact calculation. We know that something is amiss since the exact calculation fails to reproduce the normalization of the data. That is, the calculation must be multiplied by a factor of ~1.26 to obtain agreement with the data. Since the normalization is not a free parameter in an exact calculation, this is a problem yet to be resolved.

It is interesting to note that the exact calculation in Ref. 2 also had to be multiplied by a similar constant (1.30) to fit the data of that work. The normalization of the data in Ref. 2 agrees with our normalization to within 7% for the cross section integrated over the fsi peak, and to better than 2% in the proton energy regions 8.0 to 9.0 MeV and 9.0 and 10.0 MeV. Therefore, although the calculations of Ref. 2 were quite different from the exact calculations of Ref. 18, both arrive at the same normalization which disagrees by ≈26% with experiment.

The difficulties with the exact calculations may be explained by their particular treatment of off-energy-shell effects in the nucleon-nucleon interaction, by the assumption of charge independence of the interaction, or by their truncation to $S$-wave interactions. Despite the large amount of work done on the first of these problems, the effects of differing off-shell behaviors[23] have been investigated almost exclusively for kinematically complete experimental geometries which (1) do not average over unobserved particles as in our experiment, or (2) do not pertain to the region of phase space investigated here, where the proton has nearly all the energy. It would be worthwhile to fill these gaps in the theoretical analysis. The difference between hybrid calculations (where the charge dependence is only in the inhomogeneous term) and fully charge-dependent calculations has been shown[24] to be important in the magnitude of the fsi peak for a kinematically complete geometry. Since the peak shape as well as its magnitude in our geometry might be changed by inclusion of charge dependence, further calculations should include the full charge dependence. Extending the calculations to higher partial waves appears possible[25] but difficult. If higher partial waves are important

at $E_n = 14$ MeV, one would naively think that they should have their greatest effect at the very forward angles investigated in this experiment. We hope these new data will stimulate more detailed calculations for this region of phase space.

We take pleasure in thanking B. Tuckey and B. Pohl for their considerable assistance in this work. We are most grateful to W. M. Kloet for providing results of his exact calculations and to J. C. Davis for stimulating conversations.

---

*Work performed under the auspices of the U. S. Energy Research and Development Administration, W-7405-Eng-48.

[1]J. C. Davis, J. D. Anderson, S. M. Grimes, and C. Wong, Phys. Rev. C 8, 863 (1973).
[2]S. Shirato, K. Saitoh, N. Koori, and R. T. Cahill, Nucl. Phys. A215, 277 (1973).
[3]B. Kühn, Sov. J. Part. Nucl. 6, 139 (1976) [Fiz. Elem. Chastits At. Yad. 6, 347 (1975)].
[4]R. C. Haight, S. M. Grimes, B. J. Tuckey, and J. D. Anderson, Bull. Am. Phys. Soc. 20, 1194 (1975); Lawrence Livermore Laboratory Report No. UCRL-77151 (unpublished).
[5]R. Booth and H. H. Barschall, Nucl. Instrum. Methods 99, 1 (1972).
[6]M. Bartle and H. O. Meyer, Nucl. Instrum. Methods 112, 615 (1973).
[7]J. F. Janni, Air Force Weapons Laboratory Report No. AFWL-TR-65-150, 1966 (unpublished).
[8]L. C. Northcliffe and R. F. Schilling, Nucl. Data A7, 233 (1970).
[9]A. C. Paul, Lawrence Berkeley Report No. UCID-3525 (unpublished).
[10]M. Bormann and I. Riehle, Z. Phys. 207, 64 (1967).
[11]J. C. Davis and J. D. Anderson, J. Vac. Sci. Technol. 12, 358 (1975).
[12]H. Bichsel, *American Institute of Physics Handbook*, coordinating editor D. E. Gray (McGraw-Hill, New York, 1972), 3rd ed., pp. 8–142.
[13]J. C. Hopkins and G. Breit, Nucl. Data, A9, 137 (1971).
[14]R. J. N. Phillips, Nucl. Phys. 53, 650 (1964).
[15]K. M. Watson, Phys. Rev. 88, 1163 (1962).
[16]A. B. Migdal, Zh. Eksp. Teor. Fiz. 28, 3 (1955) [Sov. Phys. JETP 1, 2 (1955)].
[17]S. Shirato, K. Saitoh, and N. Koori, in *Few Particle Problems in the Nuclear Interaction*, edited by I. Šlaus *et al.* (North-Holland, Amsterdam, 1973), p. 114.
[18]W. M. Kloet (private communication).
[19]W. M. Kloet and J. A. Tjon, Nucl. Phys. A210, 380 (1973).
[20]R. V. Reid, Ann. Phys. (N.Y.) 50, 511 (1968).
[21]R. A. Malfliet and J. A. Tjon, Nucl. Phys. A127, 161 (1969).
[22]R. A. Malfliet and J. A. Tjon, Ann. Phys. (N.Y.) 61, 425 (1970).
[23]M. I. Haftel, E. L. Petersen, and J. M. Wallace, Phys. Rev. C 14, 419 (1976).
[24]B. Zeitnitz, R. Maschuw, P. Suhr, W. Ebenhöh, J. Bruinsma, and J. H. Stuivenberg, Nucl. Phys. A231, 13 (1974).
[25]J. J. Benayoun, J. Chauvin, C. Gignoux, and A. Laverne, Phys. Rev. Lett. 36, 1438 (1976).